Chinese Chemical Letters 37 (2026) 111528

Contents lists available at ScienceDirect

Chinese Chemical Letters

journal homepage: www.elsevier.com/locate/cclet

Ferromagnetic filler-induced stable electrode/electrolyte interfaces for solid-state Li metal batteries

Yucheng Wang[a], Xiaodan Li[a], Xunhui Xiong[a,*], Yuancheng Chen[a], Yun Cheng[b,*], Jianhao Lin[a], Chuang Ji[a], Yingyi Yuan[a]

[a] School of Environment and Energy, Guangdong Provincial Key Laboratory of Advanced Energy Storage Materials, South China University of Technology, Guangzhou 510006, China
[b] Guangdong Saffien New Materials Co., Ltd., Qingyuan 511520, China

ARTICLE INFO

Article history:
Received 12 April 2025
Revised 25 June 2025
Accepted 1 July 2025
Available online 2 July 2025

Keywords:
Solid-state Li metal batteries
PVDF polymer electrolyte
Ferromagnetic packing
Space charge layer
Interfacial electric field

ABSTRACT

Solid polymer electrolyte (SPEs) modified by inorganic fillers has become a simple and effective strategy to improve ionic conductivity and mechanical strength. However, the uneven charge distribution at the interface of polymer electrolyte/electrode results in unstable interfaces and poor cycle performances. Herein, ferromagnetic $(La_{0.60}Sr_{0.40})_{0.95}Co_{0.20}Fe_{0.80}O_{3-\delta}$ (LSCF) has been firstly proposed as filler for PVDF-based electrolyte (PLSCF) to address these critical challenges in solid-state Li metal battery. It has been demonstrated that LSCF filler cannot only increase the ratio of amorphous phase in the polymer, but also induce the rearrangement of PVDF molecular chains under an applied external magnetic field during the preparation process, which can facilitate the generation of the β-phase and promote the dissociation of Li^+. The synthesized PLSCF electrolyte exhibits appealing physicochemical properties, including enhanced ionic conductivity (2.09×10^{-4} S/cm), reduced activation energy (0.142 eV), and improved mechanical robustness (1.286 MPa), which can contribute to a homogeneous lithium deposition on Li metal anode. Furthermore, LSCF can establish an even electric field at the PLSCF/cathode interface, which helps to weaken the space charging layer and construct a robust cathode/electrolyte interface (CEI). As a result, both solid-state Li/Li symmetric cells and $LiNi_{0.6}Co_{0.2}Mn_{0.2}O_2$/Li full cells incorporating the PLSCF electrolyte exhibit significantly improved cycling stability and rate capability. This work enriches inorganic fillers to stabilize electrode/electrolyte interface for high-performance solid-state Li metal batteries.

© 2026 Published by Elsevier B.V. on behalf of Chinese Chemical Society and Institute of Materia Medica, Chinese Academy of Medical Sciences.

Compared with commercial graphite anode, Li metal anodes demonstrate ultrahigh capacity and the lowest working potential, which show great application potential for the high-energy-density devices. However, the Li dendrite growth and even the serious safety risks prevent the practical applications in the traditional organic electrolytes, which show high volatility and high flammability [1,2]. Utilizing solid-state electrolytes can eliminate the dangers associated with leakage and enhance the overall safety and reliability of lithium metal batteries [3–7]. Among the different solid-state electrolytes, the inorganic solid electrolyte has superior ionic conductivity and ultrahigh mechanical strength. However, the poor electrode/electrolyte interface contact leads to high impedance, uneven interfacial potential distribution, and rapid growth of Li dendrites [8,9]. In sharp contrast, solid polymer electrolytes (SPEs) with good flexibility and easy processing demonstrated high compatibility with electrode, and has become a hot research topic of solid-state electrolyte. At present, various polymers have been used in solid electrolytes, including poly(ethylene oxide) (PEO) [10,11], polyacrylonitrile (PAN) [12,13], aliphatic polycarbonates (APCs) [14], polyacrylates (PAs) [15], and poly(vinylidene fluoride) (PVDF) [16,17]. Among them, PVDF-based solid electrolyte has high dielectric constant, wide operation voltage window, and excellent thermal stability and electrochemical stability. However, PVDF-based polymer electrolytes still face several inherent limitations, including excessive crystalline domains, inadequate lithium-ion mobility, compromised mechanical properties, and unsatisfactory ionic conductivity under ambient conditions [18–20]. Especially when paired with high-voltage cathodes, residual *N*,*N*-dimethylformamide (DMF) and Li salts in the electrolyte trigger severe interfacial side reactions [21]. These reactions can promote the formation of Li dendrite at the anode/electrolyte interface and thickening of CEI layer at the cathode/electrolyte in-

* Corresponding authors.
E-mail addresses: esxxiong@scut.edu.cn (X. Xiong), chengerr@126.com (Y. Cheng).

https://doi.org/10.1016/j.cclet.2025.111528
1001-8417/© 2026 Published by Elsevier B.V. on behalf of Chinese Chemical Society and Institute of Materia Medica, Chinese Academy of Medical Sciences.

terface, leading to rapid impedance growth, declining Coulombic efficiency, and ultimately premature cell failure [22].

The incorporation of inorganic fillers into PVDF-based polymer matrices has emerged as a widely adopted approach for developing high-performance composite solid electrolytes (CSEs). The inorganic fillers can build a cross-linked structure with polymer matrix to enhance the mechanical properties, break the regularity of molecular chains, leading to a decreased crystallinity and increased ionic conductivity [23,24]. For example, the use of CTAB-functionalized montmorillonite has developed as an effective filler for PVDF-based composite electrolytes, in which the filler can establish efficient lithium-ion conduction pathways, and the polymer electrolyte can deliver an enhanced ionic conductivity of 3.44×10^{-4} S/cm [25]. Zhang *et al.* demonstrated that $Li_{6.4}La_3Zr_{1.4}Ta_{0.6}O_{12}$ (LLZTO) filler can induce the dehydrofluorination of PVDF, which can increase the amorphous regions in PVDF and accelerates lithium ions migration, resulting in significantly enhanced electrochemical performances [26]. More recently, the uneven charge distribution at the interface of polymer electrolyte/electrode has been demonstrated to induce the heterogeneous transport of ions, which has a detrimental impact on the cycle stability of the solid-state battery [27,28]. Thereafter, $BaTiO_3$-$Li_{0.33}La_{0.56}TiO_{3-x}$ (LLTO) nanowires prepared by electrospinning process have been proposed as inorganic filler to prepare high-performance CSEs, in which ferroelectric $BaTiO_3$ can alleviate the space charge layer of the composite electrolyte and dissociate more Li^+, while LLTO can provide additional transfer channels for Li^+ [29]. Liu *et al*. demonstrated that $LiNbO_3$, a ceramic material with high dielectric constant, can be polarized and then generate an internal electric field under an applied electric field, which can enhance distribution uniformity of the electric field around the PVDF electrolyte when it was used as a filler [30]. Therefore, it is necessary to explore more advanced fillers that can stabilize electrode/electrolyte interfaces for superior solid-state Li metal batteries.

Herein, ferromagnetic $(La_{0.60}Sr_{0.40})_{0.95}Co_{0.20}Fe_{0.80}O_{3-\delta}$ (LSCF) with a perovskite structure has been firstly developed as a filler for PVDF-based solid electrolyte. Except for enhancing the mechanical strength and increasing the amorphous regions in PVDF, LSCF filler can induce the rearrangement of PVDF molecular chains and promote the formation of a higher proportion of the high-dielectric β-phase under the external magnetic field during the preparation process. This structural transformation can increase the number of mobile Li^+ ions and enhance high ionic conductivity, which can effectively inhibit the formation of Li dendrite on surface of Li metal anode. Moreover, the incorporation of LSCF particles effectively reduces the interfacial potential at the PLSCF electrolyte/cathode, promoting the formation of a stable electrolyte/cathode interphase (CEI) that enables rapid and uniform lithium-ion insertion/extraction during cycling. As a result, the designed composite electrolyte with 5 wt% LSCF demonstrates superior electrochemical properties with high ionic conductivity (2.0×10^{-4} S/cm at 25 °C) and ultralow activation barrier of 0.142 eV. The composite electrolyte enables stable Li plating/stripping in symmetric cells for 1400 h at 0.1 mAh/cm^2. Besides, the NCM622/Li full cells employing the composite electrolyte exhibit exceptional cycling performance with 91.6% capacity retention after 360 cycles at 0.2 C and 92.9% after 135 cycles at 0.5 C under ambient conditions. This study proposes a novel internal field modulation strategy for designing high-performance CSEs with enhanced interfacial stability.

LSCF nanoparticles (Fig. S1 in Supporting information) were subjected to ball milling and ultrasonic treatment in a DMF solution to obtain a uniformly dispersed LSCF-DMF composite slurry. Subsequently, PVDF powder and LiFSI were added into the LSCF-DMF composite slurry, and the CSE can be obtained *via* solution casting method after a thorough mixing. The as-prepared CSE membranes with different LSCF contents of 2.5 wt%, 5 wt%, and 10 wt% were labeled as PLSCF-2.5, PLSCF-5, and PLSCF-10, respectively (Fig. S2 in Supporting information). For comparison, the traditional PVDF electrolyte was also prepared under the identical experimental conditions except the addition of LSCF particles.

The morphological differences between PVDF and PLSCF electrolyte films were systematically investigated through scanning electron microscopy (SEM) characterization. As illustrated in Figs. 1a and b, the PVDF matrix displays an open, porous architecture with poor particle packing, while the PLSCF composite shows a consolidated, densely packed microstructure with minimal void space. Compared with a large thickness of 202 μm for the pure PVDF film, the PLSCF film further reveals a compact structure with small particle sizes and a reduced thickness of approximately 160 μm, as displayed in the cross-sectional SEM image in Fig. S3 (Supporting information). This structural difference can be attributed to the role of LSCF particles in providing additional nucleation sites during PVDF crystallization [31]. Meanwhile, the surface EDS mappings in Fig. 1c demonstrate LSCF particles are uniformly distributed within the whole PVDF matrix for the PLSCF-5 electrolyte, which is critically important to ensure the stability of the electrolyte membrane. However, when the LSCF content reaches to 10 wt%, the filler exhibits significant agglomeration (Fig. S4 in Supporting information), leading to the formation of dense clusters in the PLSCF-10 membrane. With its dense and uniform micro-structure, the PLSCF-5 electrolyte demonstrates significantly enhanced mechanical strength, exhibiting a tensile strength of 1.286 MPa (Fig. 1d), which is nearly double that of pure PVDF electrolyte (0.673 MPa). Furthermore, the dense structure and reduced thickness provide a continuous ion transport pathway, thereby contributing to an improved ionic conductivity [32]. The atomic force microscopy (AFM) characterization reveals the PLSCF-5 electrolyte surface exhibits significantly reduced roughness (15.4 nm, Fig. 1e) compared to the PVDF electrolyte (66.9 nm, Fig. 1f). The flat and homogeneous surface morphology enhances the electrolyte/electrode interfacial contact, thereby facilitating convenient ion transport across the interface [33]. To elucidate the influence of LSCF filler on the PVDF matrix, systematic X-ray diffraction (XRD) and Fourier transform infrared spectroscopy (FTIR) analyses were conducted on both pristine PVDF and PLSCF membranes with varying LSCF loadings. The XRD patterns in Fig. 2a indicate that the ball milling process in DMF will not alter the crystal structure of LSCF, which can fully retain the initial structural integrity. After introducing the filler, two obvious peaks located at 32.8° and 58.7° corresponding to LSCF can be observed in the PLSCF electrolytes. No any peaks of impurity phase are appeared, suggesting that LSCF remains chemically stable in the presence of both PVDF and LiFSI. It is worth noting that the addition of LSCF can greatly broaden the characteristic PVDF peaks (Fig. 2b), indicating a reduced crystallinity of PVDF. Thus, Li^+ can more efficiently rely on the chain segment motion for transfer in the amorphous region [34,35]. In the FTIR spectrum (Fig. 2c), all the characteristic peaks of the PVDF-based polymer electrolyte membrane experience no shift, indicating that LSCF is likely to be physically mixed with other components. However, the characteristic peaks at 1275 and 840 cm^{-1} show reduced intensities, resulting from LSCF-induced amorphization of the PVDF polymer matrix. To more accurately reflect the changes, the detailed phases in the different PVDF-based electrolytes were quantified from the FTIR spectroscopies. Generally, α-phase is usually identified by characteristic absorption bands at 764 and 976 cm^{-1}, while the β-phase is associated with bands at 840 and 1275 cm^{-1} in the FTIR spectroscopy [36]. Therefore, the β-phase content can be calculated *via* using the Beer-Lambert law [37,38], which experiences a gradual increase with the increasing of LSCF content in the CPEs (Fig. S5 in Supporting information). Specifically, the β-phase content in

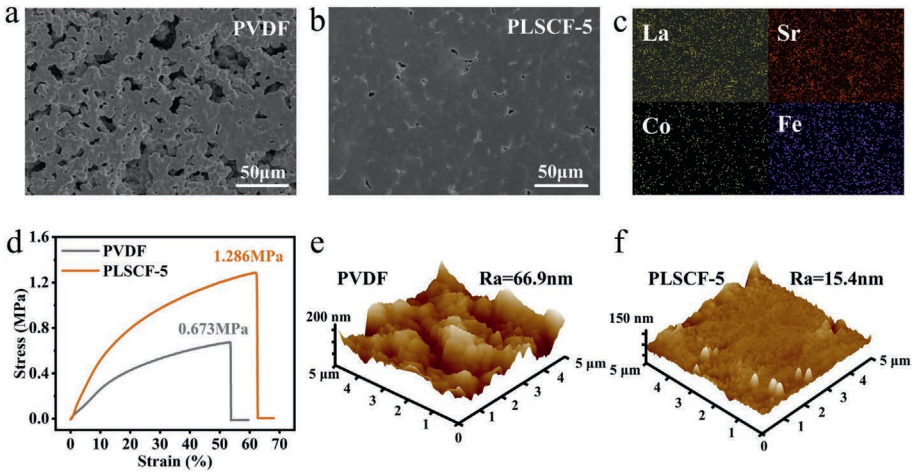


Fig. 1. SEM images showing (a) PVDF and (b) PLSCF-5 electrolyte surfaces. (c) EDS elemental mappings of La, Sr, Co and Fe in the PLSCF-5 electrolyte. (d) Stress–strain curves of PVDF and PLSCF-5 electrolytes. AFM morphology images of (e) PVDF and (f) PLSCF-5.

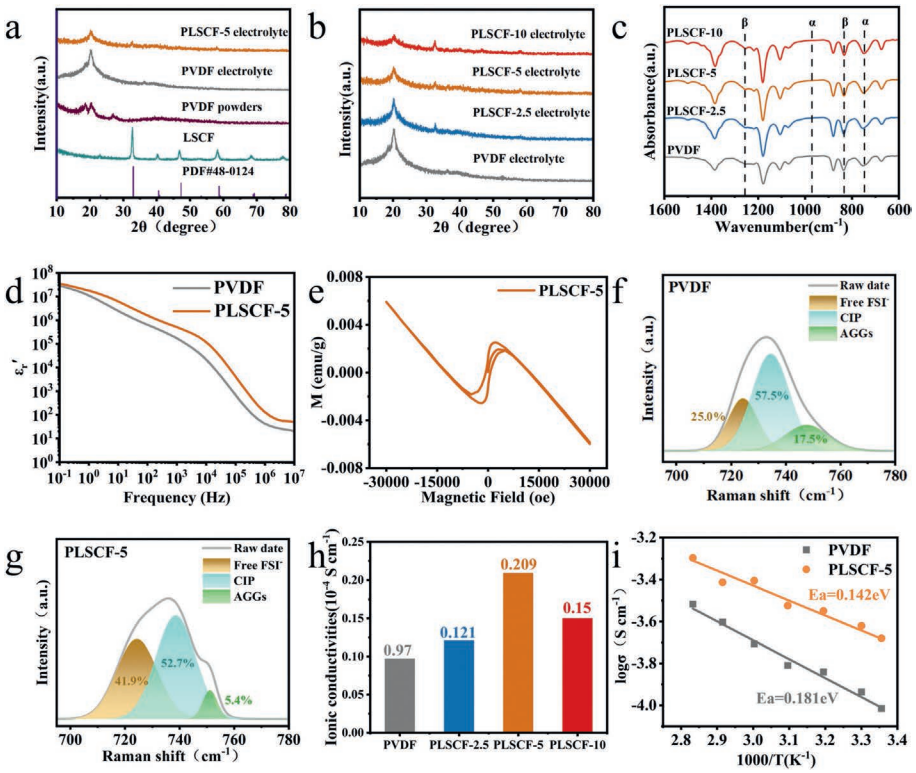


Fig. 2. (a) XRD patterns of LSCF filler, PVDF powder, and PVDF/PLSCF-5 electrolyte film. (b) XRD patterns PVDF electrolyte with various LSCF contents. (c) FTIR spectra of PVDF and PLSCF-2.5, 5, 10 electrolytes. (d) Real part (ε_r') of relative permittivity as a function of frequencies at 300 K temperature for PVDF and PLSCF-5 polymer films. (e) MH loop for PLSCF-5 at 300 K temperature. Raman spectra of (f) PVDF and (g) PLSCF-5 electrolyte. (h) Ionic conductivities of PLSCF-based electrolytes with different percentages of LSCF at room temperature. (i) Arrhenius plots of the pure PVDF electrolyte and PLSCF-5 electrolyte.

the pure PVDF electrolyte is 48.1 %, and it climbs to 54.5 %, 55.1 %, and 56 % for PLSCF-2.5, PLSCF-5, and PLSCF-10 electrolytes, respectively. Similar phenomenon can be confirmed in broadband dielectric spectroscopy (BDS) measurements (Fig. 2d), in which PLSCF-5 electrolyte shows a higher dielectric property of than pure PVDF electrolyte, indicating a higher amount of β-phase in PLSCF-5. To explore the reason for the enhanced amount of β-phase in PLSCF-5 electrolyte, the magnetization (M) *versus* magnetic field (H) behavior of ferromagnetic and at 300 K was characterized (Fig. 2e). The pure PVDF electrolyte demonstrates its diamagnetic nature, however, PLSCF-5 electrolyte shows magnetic property after the incorporation of LSCF. Under an applied external magnetic field during the solution-casting process, the strong magnetic field from LSCF can create internal stress at the interfaces of LSCF/PVDF matrix and facilitate the alignment of PVDF molecular chains, resulting in a further improvement of β-phase [39]. The increase of β-phase content in PVDF matrix induced by LSCF significantly improved the dissociation efficiency of lithium salts and promoted ion transport in electrolyte [40].

Raman spectroscopy was also performed to elucidate more effect of LSCF on the structure of PLSCF-5 membranes (Figs. 2f and g). Three distinct vibrational modes of FSI^- at 724, 738, and 751 cm^{-1} in both PVDF and PLSCF-5 films reveal three kinds of ionic states, which can attributed to free FSI^- anions, contact ion

pairs (CIPs) (FSI^- coordinated to single Li^+ cation), and aggregates (AGGs) (FSI^- coordinated to more than one Li^+ cations), respectively [29]. The introduction of LSCF induces notable effect of the ionic dissociation states. Specifically, the ratios of CIPs experience a slight decrease from 57.5 % to 52.7 %, while AGGs experience a substantial reduction from 17.5 % to 5.4 %. Notably, the ratios of free FSI^- in the PLSCF-5 electrolyte jumps to 41.9 % from 25.0 %, resulting in the formation of more mobile Li^+ and a higher ionic conductivity. To determine the ionic conductivity values, AC impedance spectroscopy measurements were performed on symmetric cells fabricated with PLSCF electrolytes. As shown in Fig. 2h and Fig. S6 (Supporting information), the ionic conductivity of the PVDF electrolyte (9.66×10^{-5} S/cm at 25 °C) can be significantly enhanced upon the addition of LSCF, with PLSCF-5 exhibiting the highest ionic conductivity (2.09×10^{-4} S/cm at 25 °C). The enhanced ionic conductivity can be verified by the activation energy (E_a) of ion migration, which can be calculated from the Arrhenius plots. Fig. 2i demonstrates that the PLSCF-5 electrolyte achieves a significantly reduced activation energy ($E_a = 0.142$ eV) compared to the PVDF electrolyte ($E_a = 0.181$ eV). It is worth noting that the significantly reduced residual DMF content observed in PLSCF-5 relative to PVDF (Fig. S7 in Supporting information) demonstrates that the enhanced ionic conductivity and reduced E_a of PLSCF-5 are primarily attributed to the introduction of LSCF, which can increase amorphous region, enhance the content of β-phase and provide more free FSI^- in the solid-state electrolyte. However, the ionic conductivity begins to decline as the LSCF content further increases to 10 %, which is largely due to filler aggregation and increased interparticle impedance [41]. In addition, the PLSCF electrolyte demonstrates an expanded electrochemical stability window up to 4.5 V (Fig. S8 in Supporting information), representing a 0.1 V improvement over the pure PVDF electrolyte (4.4 V) and confirming its enhanced compatibility with high-nickel layered oxide cathodes.

Given the unique benefits of LSCF filler, the electrochemical performances of the PVDF-based films were studied. As shown in Fig. 3a, the Li/PLSCF-5/Li cell achieves a high critical current density of 2.2 mA/cm^2, three times enhancement when compared to the PVDF-based system (0.6 mA/cm^2). The Li/PLSCF-5/Li cell maintains exceptional cycling stability over 1400 h at 0.1 mA/cm^2 and 0.1 mAh/cm^2 with minimal overpotential variation (Fig. 3b), whereas the PVDF-based counterpart fails suddenly after just 264 h of operation due to internal short-circuiting. Meanwhile, when the current density was set as 0.3 mA/cm^2, the PLSCF-5 electrolyte can keep a stable cycling for 650 h (Fig. 3c), dramatically outperforming the PVDF electrolyte (93 h). Compared with pure PVDF electrolyte, the PLSCF-5 electrolyte possesses a superior ability to suppress Li dendrite growth especially at high current densities. The sharp difference of the cycle performances can be verified by the SEM images of the cycled Li metal. The cycled Li anode in the PLSCF-5-based symmetric cell exhibits a smooth, dendrite-free morphology, as confirmed by post-cycling characterization (Fig. 3d). In contrast, the PVDF-based electrolyte leads to extensive Li dendrite formation on the metal anode after 50 cycles, as clearly evidenced by the surface morphology in Fig. 3e. Additionally, AFM characterization of cycled Li metal anodes reveals a dramatic difference in surface morphology between the two electrolyte systems. The PLSCF-5 electrolyte produces remarkably smooth surfaces with a roughness of just 2.63 nm (Fig. S9 in Supporting information), in stark contrast to the rough Li deposits with an average roughness of 192.4 nm formed with the PVDF electrolyte, demonstrating its superior ability to regulate Li deposition. Therefore, the PLSCF-5 electrolyte can more effectively homogenize the Li deposition.

X-ray photoelectron spectroscopy (XPS) analysis was conducted to characterize the chemical composition of the solid-electrolyte interphase (SEI) layer formed on the lithium anode following cycling in Li/Li symmetric cells. The C 1s XPS spectrum (Fig. 3f) reveals characteristic peaks at 285.8 and 288.6 eV, which are assigned to C–O and C=O bonds, respectively, confirming the formation of Li_2CO_3 in the SEI layer [34]. XPS analysis reveals reduced peak intensities for C=O (288.6 eV) and C–O (285.8 eV) bonds in the PLSCF-5 electrolyte compared to PVDF, demonstrating decompositions of both DMF solvent and PVDF polymer chains are significantly suppressed at the electrode/electrolyte interface. The F 1s XPS spectrum (Fig. 3g) exhibits two characteristic peaks at 687.7 and 684.8 eV, corresponding to the C-F bond in FSI^- and LiF, respectively, confirming the presence of both decomposition products and intact salt anions at the interface [42]. In the S 2p spectrum (Fig. 3h), three distinct peaks are observed at 167.3, 168.8, and 170.1 eV, corresponding to SO_3^-, SO_2F^-, and NSO_2^- species derived from LiFSI, respectively [30]. These results suggest that the SEI layer formed on cycled Li metal is predominantly generated through the decomposition reactions of LiFSI, PVDF and DMF. XPS analysis demonstrates superior interfacial stability of the PLSCF-5 electrolyte compared to PVDF, with significantly reduced evidence of side reactions at the lithium electrode interface.

Given the demonstrated the exceptional interfacial stability of the PLSCF-5 electrolyte with lithium metal anodes, we fabricated solid-state NCM622/Li full cells to assess practical viability. The enhanced ionic conductivity of PLSCF-5 translates directly to improved electrochemical performance, with the NCM622/PLSCF-5/Li cells demonstrating superior rate capability across multiple current densities (Fig. 4a). The NCM622/PLSCF-5/Li cell exhibits excellent rate capability, delivering discharge capacities of 166.7, 157.8, 151.8, 143.4, 126.5, and 97.7 mAh/g at progressively increasing current rates from 0.1 C to 5 C, respectively. As the current rate was reset as 0.1 C, the cell can almost fully return to the initial discharge capacity, demonstrating outstanding cycling reversibility. Besides, the solid-state NCM622/PLSCF-5/Li full cells exhibit remarkable cycling stability with 91.6 % capacity retention after 360 cycles at 0.2 C (Fig. 4b). This performance significantly outperforms the NCM622/PVDF/Li cells, which show rapid capacity decay attributable to severe interfacial degradation. Besides, the NCM622/PLSCF-5/Li cells can demonstrate remarkable cycling stability at 0.5 C with 92.9 % capacity retention over 135 cycles, in stark contrast to the NCM622/PVDF/Li counterparts which undergo premature failure due to short-circuiting at the 23rd cycle (Fig. 4c). The overlapped cyclic voltammetry (CV) curves from the second cycle further corroborate the NCM622/PLSCF-5/Li full has a higher reversibility than that of NCM622/PVDF/Li cell (Figs. 4d and e). These findings indicate that the PLSCF-5 electrolyte exhibits exceptional interfacial stability with both the NCM622 cathode, highlighting its potential for advanced solid-state battery applications.

To explore the origin of the enhanced full-cell performances, the interface of NCM622 and PLSCF-5 electrolyte was further studied after 50 cycles at 0.2 C. Firstly, the AFM characterization (Fig. S10 in Supporting information) shows the cycled PLSCF-5 electrolyte exhibits an extremely low roughness value of 18 nm, significantly smoother than the cycles PVDF electrolyte ($R_a = 154$ nm). Besides, the potential distribution at the NCM622/electrolyte interface was also investigated using Kelvin probe force microscopy (KPFM) (Figs. 5a and b). The smooth surface of PLSCF-5 electrolyte effectively mitigates localized charge accumulation at the electrolyte/cathode interface, resulting in significantly more uniform potential distribution compared with pure PVDF electrolyte. Specifically, the potential distribution analysis in Figs. 5c and d demonstrates a markedly reduced interfacial potential at the NCM622/PLSCF-5 interface (45.3 mV) compared with the NCM622/PVDF interface (132.2 mV), reflecting improved interfacial stability. This demonstrates that the PLSCF-5 electrolyte can suppresses space charge layer formation at the interface, thereby facilitating Li^+ transport. Moreover, the structure of the cycled NCM622 was also studied. The NCM622 particles cycled in NCM622/PLSCF-

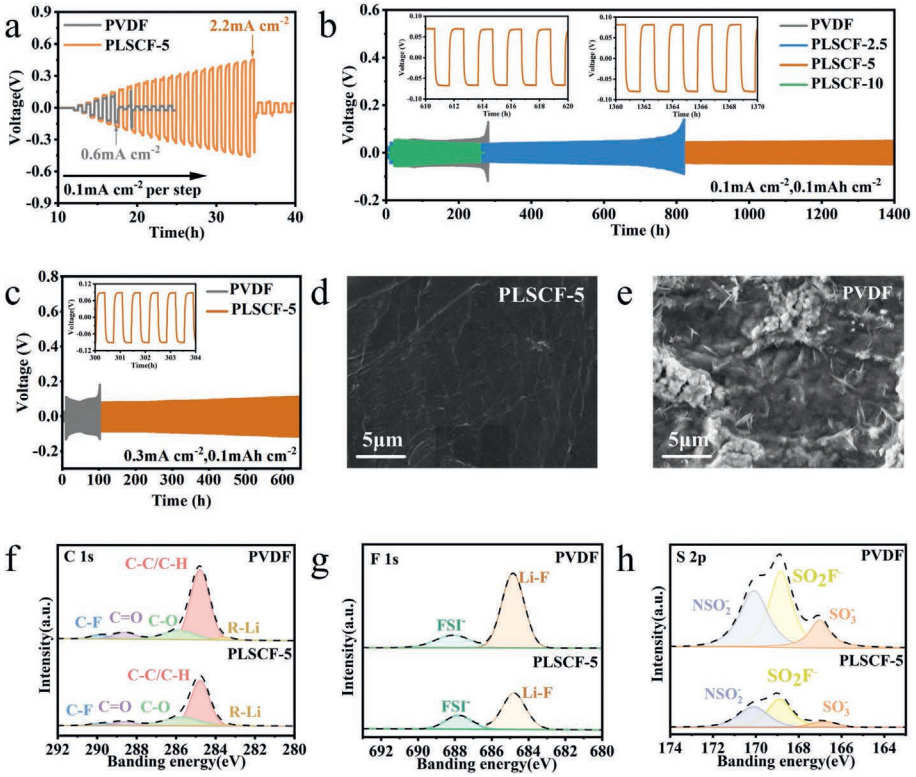


Fig. 3. (a) CCD performance of Li symmetric cells with PVDF and PLSCF-5 electrolytes. Electrochemical cycling stability of Li symmetric cells employing (b) PVDF and (c) PLSCF-5 electrolytes under galvanostatic conditions at 0.1 and 0.3 mA/cm^2 (0.1 mAh/cm^2 capacity limit). Post-cycling Li metal morphology after 50 cycles at 0.1 mA/cm^2 with (d) PVDF and (e) PLSCF-5 electrolytes. XPS analysis of cycled Li anodes: (f) C 1s, (g) F 1s, (h) S 2p spectra for PVDF and PLSCF-5 electrolytes.

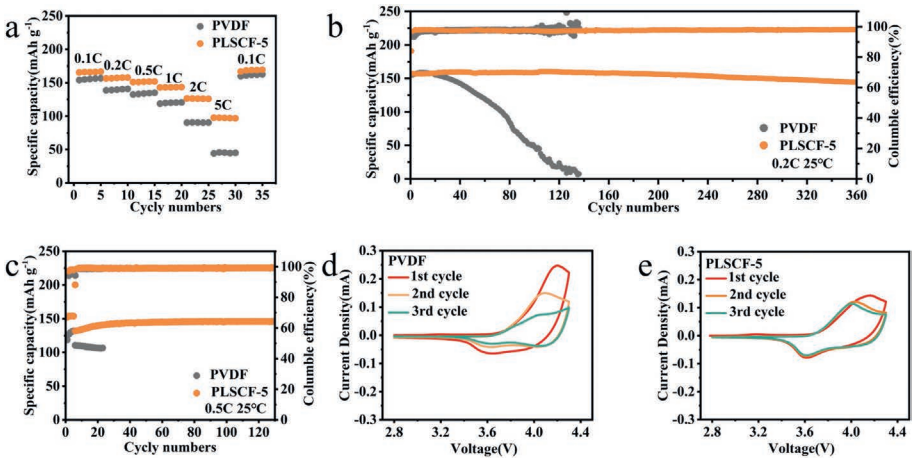


Fig. 4. (a) Rate capability comparison of NCM622/Li cells employing PVDF *versus* PLSCF-5 electrolytes. (b) 0.2 C and (c) 0.5 C cycling performance of NCM622/Li cells with PVDF *versus* PLSCF-5 electrolytes. Cyclic voltammetry profiles comparing NCM622/Li cells with PVDF (d) and PLSCF-5 (e) electrolytes at 2.8–4.3 V.

5/Li cells show a much thinner surface layer (~4 nm) consisting of both rock-salt phase (site A) and mixed phase (site B) after 50 cycles (Fig. 5e), compared to those cycled in NCM622/PVDF/Li cells (~11 nm, Fig. 5f). Therefore, PLSCF-5 electrolyte effectively suppresses phase transformation on the surface of NCM622. The results confirm that LSCF filler in PVDF electrolytes can reduce space charge effects and minimize interfacial side reactions between electrodes and electrolytes.

In this work, ferromagnetic LSCF has been firstly proposed as filler for PVDF polymer electrolytes to enhance the compatibility at the interface polymer electrolyte/electrode. The experimental data demonstrate that the LSCF filler can enhance the mechanical strength, increase the amorphous regions in PVDF and induce the rearrangement of PVDF molecular chains and promote the formation of a higher proportion of the high-dielectric β-phase. Thus, the composite electrolyte containing 5 wt% LSCF demonstrates superior ionic transport properties, achieving both high ionic conductivity (2.09×10^{-4} S/cm at 25 °C) and remarkably low activation energy (0.142 eV), which contribute to uniform lithium deposition morphology and effective dendrite suppression during cycling. Furthermore, the LSCF filler incorporation not only suppresses interfacial side reactions and reduces cathode/electrolyte potential but also facilitates the development of a robust CEI layer, ensuring efficient and homogeneous Li^+ migration throughout extended cycling. The PLSCF-5 electrolyte enables exceptional cycling stability in both Li/Li symmetric cells and NCM622/Li full cells, along with significantly improved rate capability. Our study demonstrates that the use of ferromagnetic fillers to regulate the internal interface

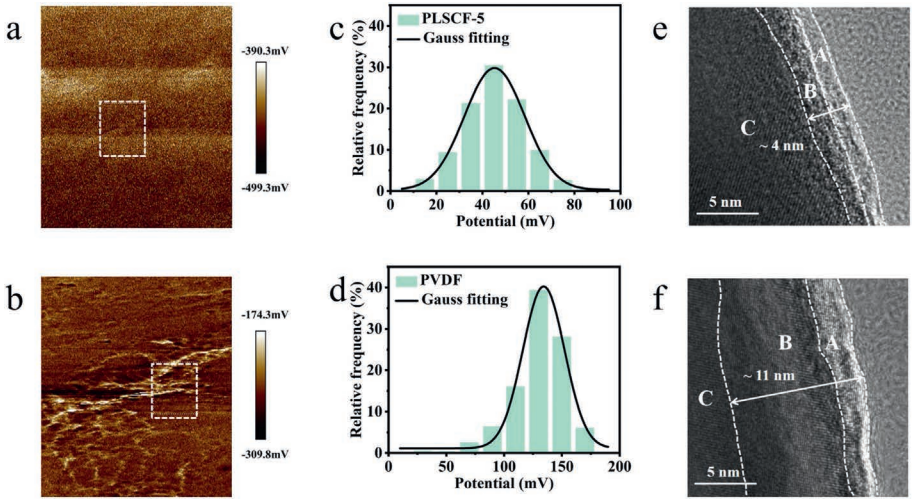


Fig. 5. Interfacial potential distribution of NCM622 with (a) PVDF and (b) PLSCF-5 electrolytes. Gaussian distribution of interfacial potentials for NCM622 with (c) PVDF and (d) PLSCF-5 electrolytes. Post-cycling TEM characterization of NCM622 cathodes after 50 cycles at 0.2 C with (e) PVDF and (f) PLSCF-5 electrolytes.

stability represents a simple and efficient strategy for developing high-performance solid-state batteries.

CRediT authorship contribution statement

Yucheng Wang: Writing – original draft, Methodology, Formal analysis, Conceptualization, Validation, Investigation, Data curation. **Xiaodan Li:** Investigation, Methodology, Conceptualization. **Xunhui Xiong:** Writing – review & editing, Project administration, Supervision, Conceptualization. **Yuancheng Chen:** Investigation. **Yun Cheng:** Supervision. **Jianhao Lin:** Methodology. **Chuang Ji:** Methodology. **Yingyi Yuan:** Investigation.

Declaration of competing interest

The authors declare that they have no known competing financial interests or personal relationships that could have appeared to influence the work reported in this paper.

Acknowledgments

The authors gratefully acknowledge the financial support from the National Natural Science Foundation of China (No. 52322406), the Natural Science Foundation of Guangdong Province, China (Nos. 2024A1515010827, 2022A1515010231) and the Double Thousand Plan in Jiangxi Province (No. jxsq2023101061).

Supplementary materials

Supplementary material associated with this article can be found, in the online version, at doi:10.1016/j.cclet.2025.111528.

References

[1] C. Chen, Q. Liang, G. Wang, et al., Adv. Funct. Mater. 32 (2022) 2107249.
[2] C. Ji, Q. Zhou, Y. Yuan, et al., Energy Environ. Sci. 17 (2024) 4273–4282.
[3] H. Chen, M. Zheng, S. Qian, et al., Carbon Energy 3 (2021) 929–956.
[4] Y. Wang, J. Wang, J. Nai, et al., Chin. Chem. Lett. 35 (2024) 108510.
[5] K. Yang, L. Li, Y. Xiao, et al., Chin. Chem. Lett. 35 (2024) 108451.
[6] X. Li, Q. Liu, Y. Wang, et al., Small 21 (2025) 2411104.
[7] X. Zhang, S. Wang, C. Xue, et al., Adv. Mater. 31 (2019) 1806082.
[8] Y. Zhao, Y. Zhang, D. Gosselink, et al., Membranes 2 (2012) 553–564.
[9] M. Hong, Q. Dong, H. Xie, et al., ACS Energy Lett. 6 (2021) 3753–3760.
[10] M. Zhang, M.B. Gomes, A. Yusuf, et al., Eur. Polym. J. 215 (2024) 113246.
[11] Q. Song, Y. Zhang, J. Liang, et al., Chin. Chem. Lett. 35 (2024) 108797.
[12] R. Yin, Z. Zhang, C. Shi, et al., ACS Appl. Mater. Interfaces 16 (2024) 60142–60150.
[13] D. Kumar, S. Mukherjee, A. Das, J. Appl. Polym. Sci. 141 (2024) e55552.
[14] Z. Zhang, Y. Ren, J. Liang, et al., Energy Storage Mater. 71 (2024) 103667.
[15] G. Lu, Y. Zhang, J. Zhang, et al., Carbon Energy 5 (2023) e287.
[16] S. Khurana, S. Negi, A. Chandra, Polym. Test. 96 (2021) 107118.
[17] G. Xi, M. Xiao, S. Wang, et al., Adv. Funct. Mater. 31 (2021) 2007598.
[18] Y. Wu, Y. Li, Y. Wang, et al., J. Energy Chem. 64 (2022) 62–84.
[19] X. Li, Y. Wang, Q. Zhou, et al., J. Mater. Chem. A 12 (2024) 7645–7653.
[20] S. Zhou, S. Zhong, Y. Dong, et al., Adv. Funct. Mater. 33 (2023) 2214432.
[21] Z. Wang, S. Xie, X. Gao, et al., Chin. Chem. Lett. 34 (2023) 108151.
[22] X. An, Y. Liu, K. Yang, et al., Adv. Mater. 36 (2024) 2311195.
[23] S. Liu, W. Liu, D. Ba, et al., Adv. Mater. 35 (2023) 2110423.
[24] Q. Zhou, J. Ma, S. Dong, et al., Adv. Mater. 31 (2019) 1902029.
[25] L. Li, Y. Shan, X. Yang, Mater. Today Commun. 26 (2021) 101910.
[26] X. Zhang, T. Liu, S. Zhang, et al., J. Am. Chem. Soc. 139 (2017) 13779–13785.
[27] K. Li, J. Wang, Q. Shen, et al., Adv. Energy Mater. 14 (2024) 2400956.
[28] S. Li, S.Q. Zhang, L. Shen, et al., Adv. Sci. 7 (2020) 1903088.
[29] P. Shi, J. Ma, M. Liu, et al., Nat. Nanotechnol. 18 (2023) 602–610.
[30] X. Liu, B. Wen, G. Zhong, et al., Sci. China Mater. 67 (2024) 1947–1955.
[31] T.U. Patro, M.V. Mhalgi, D.V. Khakhar, et al., Polymer 49 (2008) 3486–3499.
[32] Y. Zhu, F. Wang, L. Liu, et al., Energy Environ. Sci. 6 (2013) 618–624.
[33] Y. Jin, X. Zong, X. Zhang, et al., J. Power Sources 501 (2021) 230027.
[34] Y. Shan, L. Li, X. Yang, ACS Appl. Energ. Mater. 4 (2021) 5101–5112.
[35] J. Lu, Y. Li, W. Huang, Mater. Res. Bull. 153 (2022) 111880.
[36] J.P. Serra, R.S. Pinto, J.C. Barbosa, et al., Sustain. Mater. Technol. 25 (2020) e00176.
[37] R. Mishra, S.K. Singh, H. Gupta, et al., Energy Fuels 35 (2021) 15153–15165.
[38] P. Martins, A.C. Lopes, S. Lanceros-Mendez, Prog. Polym. Sci. 39 (2014) 683–706.
[39] S. Jiang, H. Wan, H. Liu, et al., Appl. Phys. Lett. 109 (2016) 102904.
[40] W. Guo, C. Tan, K. Shi, et al., Nanoscale 10 (2018) 17751–17760.
[41] F. Chen, M. Jing, H. Yang, et al., Ionics 27 (2021) 1101–1111.
[42] J. Jiang, A. Wang, W. Wang, et al., J. Energy Chem. 46 (2020) 114–122.